(Received 12 January 2026, Accepted 31 March 2026, Scheduled 1 May 2026)

Ultra Wideband Printed Antenna with an Energy Harvesting Rectifier Circuit Design for 2.45 GHz (ISM) Applications

Hesham A. El-Hakim[1,*], Mohamed Morgan[1], Hesham A. Mohamed[2], and Mohamed Hussien Moharam[1]

[1]*Electronics & Commuication Department, College of Engineering, Must University for Science and Technology, Giza, Egypt*
[2]*Microstrip Department, Electronics Research Institute, Nozha, Cairo 11843, Egypt*

ABSTRACT: Nowadays, a planar antenna for engineering and scientific fields is necessary for state-of-the-art energy harvesting applications. In this study, we present an ultra-wideband (UWB) microstrip antenna for different radio frequency (RF) applications, besides an energy harvesting rectifier section to charge operational low-power devices at 2.45 GHz. This antenna is used as a broadband antenna starting from 2.1 up to 7 GHz for worldwide interoperability of microwave access (WiMAX), wireless local area networks (WLAN), and ISM applications. It also covers frequency bands of 3.3–3.8 and 4.8–5 GHz for 5G mobile systems' upper and lower frequency bands, respectively. The engineered antenna comprises an octagon-shaped radiator patch, circular slots backed with a defected ground structure (DGS), and finally, a copper-reflected layer at a distance of 26 mm from the radiator patch. It is fabricated on an FR4 dielectric substrate with overall dimensions of $47 \times 47 \times 1.6\,\text{mm}^3$. The antenna is engineered using the Microwave Studio Computer Simulation Technology (CST) electromagnetic (EM) simulator. It was tested using the ZVA 67 Rohde & Schwarz vector network analyzer (VNA). The measurement results demonstrate that the designed antenna fulfills a broad bandwidth with input reflection coefficient values (S_{11}) ≤ -10 dB from 2.1 to 7 GHz, besides three frequency resonances at 2.45, 3.8, and 5.88 GHz, respectively. A rectifier circuit modeling for the proposed design has been executed using the Advanced System (ADS) toolbox to implement an equivalent circuit for the manufactured antenna at the ISM band (2.45 GHz). The peak conversion efficiency for the designed rectenna is 98.5% at -10 dBm and 95.8% at 0 dBm under the load resistance of 50 kΩ. The fabricated prototype achieves omnidirectional and/or bidirectional measured radiation patterns in both E and H planes with stable high peak gain values of nearly 8 dB within the entire bandwidth. A comparison between the proposed antenna's prototype and the other presented in recent literature is reported to validate the design consistency.

1. INTRODUCTION

Self-powered electronics have garnered a lot of attention lately in engineering and scientific fields, including wireless sensor networks, smart buildings, and the Internet of Things (IoT). The need for these energy-collecting devices is rising because of the maintenance issues with conventional battery-operated systems, which necessitate regular battery replacement and charging. A large amount of energy is wasted during the power conversion process that charges PDAs, cell phones, and other sensors or actuator components. This problem can be lessened by harvesting ambient energy, which is widely accessible and can be obtained in the following forms: solar ($100\,\text{mW/cm}^2$), thermal ($60\,\mu\text{W/cm}^2$), vibration ($200\,\mu\text{W/cm}^2$), and RF ($1\,\mu\text{W/cm}^2$) [1, 2].

In addition, parts used for 3G, 4G, 5G, and 6G wireless communications have achieved progress in many applications, like WLAN, GPS, Wi-Max, Wi-Fi, IR, and others. An indispensable part of contemporary wireless networking and communication systems is the antenna that allows the transmission of voice and data without cables or wires. In response, studies on antennas related to wireless communication sensors are expanding, especially for applications requiring narrow and wide bandwidths, including single, UWB, multiband, triple, and dual-band antennas. The following characteristics should be attained by the most advanced antenna technologies: portability, low cost, low profile with moderate power consumption, simplicity in design, and reduction in size. In addition to the aforementioned antenna properties, appropriate antenna design approaches are crucial for offering a compact antenna size. Nonetheless, the most often used antenna configurations at the moment are microstrip patch antennas, which are easily integrated into the printed circuit boards (PCBs) of wireless communication devices and come in a variety of sizes, geometries, and arrangements [3]. The microstrip patch antenna is generally formed by three layers; the upper one is a thin metal layer, besides two other layers, the middle is a dielectric substrate backed with a thin metal layer [4]. The leading wireless systems concerns are now on the run because of the upcoming wireless technology demands, such as large impedance bandwidth exclusively in either WLAN or WiMax applications. They are used in several bands, including (2.2 : 2.5), (3.4 : 3.6) or (4.8 : 7) GHz or individually at 2.3, 2.5, 3.3, 3.5, 5, 5.5, and 6.8 GHz frequencies [5].

In addition to antenna technologies, energy harvesting concepts have been proposed to collect energy from the surrounding environment using numerous techniques. Rectenna, a combination of rectifier and antenna, is seen to be the most encouraging technique for wireless energy harvesting. It would be a

* Corresponding author: Hesham Abd El-Hakim (hesham.fahem@must.edu.eg).

great option for low-power batteries used in alternating electrical systems. EM energy has the advantage of being available all day long, whether in urban or rural settings, indoors or outdoors. To overcome its poor power density in the environment, it requires an additional effective power-boosting device. The implementation of other harvesting methods, including RFID and the Internet of Things (IoT), is then presented in [6]. In order to convert electromagnetic (EM) radiation into direct current (DC) signals, the energy harvesting system has a rectifier circuit and a microwave antenna besides a matching unit to capture the maximum amount of energy across a wide frequency range. The development of RF energy harvesting and wireless power transfer has remarkable advancements in order to convert electromagnetic (EM) radiation into direct current (DC) signals, the energy harvesting system has a rectifier circuit and a microwave antenna, besides a matching unit to capture the maximum amount of energy across a wide frequency range. The development of RF energy harvesting and wireless power transfer has led to remarkable advancements in compact rectenna arrays to be used for small handheld devices, such as smartphones, tablets, smartwatches, and other gadgets. RF energy harvesting devices should span most communications bands, such as Bluetooth/Wi-Fi (2.4, 5.1, 5.8 GHz) and WiMAX (2.5, 3.4–3.6, 5 GHz) [7].

The DC output voltage at low input signal power is thought to be the primary parameter to measure the performance of RF harvesting systems, since the output power should be sufficient to control the electronic devices and store appropriate energy for backup processes. Inherent power losses and load impedance in the rectenna, as well as the non-linearity of the rectifier at the operating frequencies, are the utmost challenges for the cutting-edge harvesting rectenna design. A slotted planar antenna with dimensions of 18 mm × 30 mm × 1.6 mm embedded on FR4 substrate is proposed in [1]. The antenna exhibited an omnidirectional radiation pattern in the E-plane of wide coverage with an S_{11} value of nearly -40 dB at 2.45 GHz and a peak gain of 5.6 dB, whereas the measured conversion efficiency is 68% at 5 dBm input signal power. In [8], a low-profile antenna is fabricated on a biocompatible polyimide substrate with total dimensions of $25.2 \times 21.5 \times 0.053\,\text{mm}^3$ and a permittivity value of 3.4. The antenna achieved a gain value close to 3.2 dBi and a conversion efficiency of 78.2% at 2.45 GHz. According to [9], a compact antenna of dimension $50 \times 50 \times 1.6\,\text{mm}^3$ is printed on an FR4 dielectric substrate and comprises an octagonal radiator and Vicsek fractal slots backed with a DGS plane. The S_{11} measurements show that the planar structure achieves values lower than -10 dB from 2.48 to 6.7 GHz with double resonating frequencies at 3.6 and 5.3 GHz, respectively. The proposed antenna produces gain values of 2.78 and 5.32 dBi with high efficiencies of 88.5% and 84.6% besides omnidirectional radiation patterns in the H/E-plane, respectively, at the resonant frequencies. In [10] a design of a rectenna for Wi-Fi energy harvesting applications at 2.42 GHz has been considered. It comprises a rectangular patch, dual circular radiating elements, and a partial ground embedded on an epoxy FR4 substrate of 4.3 dielectric constants and a total area of $80 \times 80\,\text{mm}^2$. The proposed antenna shows $S_{11} < -10$ dB at 2.42 GHz and 3.94 dB peak gain, a peak efficiency of 78.53%, and an output voltage of 4.7 V at input power equal to 0 dBm. A coplanar waveguide (CPW) rectenna has been considered in [11] for efficient RF energy harvesting at 2.4 GHz WLAN and Bluetooth applications. Its substrate is printed on FR4 material of dimensions $(40 \times 35 \times 1.6)\,\text{mm}^3$ fed by (CPW) technology with 50 Ω transmission line (T.L.) It achieves a gain of 4.12 dBi and 66.7% conversion efficiency at 5 dBm input power and 3 kΩ load resistance. In [12], the thicknesses and dielectric constants of the three substrate layers of a triangle-shaped patch antenna from the top are, respectively, (1.27, 11.71, 1.52) mm and (2, 1, 3.66). It achieved an operating bandwidth ranging from 1.75 to 2.26 GHz with $S_{11} < -10$ dB. Its rectifier circuit consists of an HSMS-2860 Schottky diode and eleven segments of transmission lines manufactured on the top layer of a Roger 3006 dielectric substrate with 1.27 mm thickness, a loss tangent of 0.0027, and a dielectric constant value of 6.15. The resulting DC output power was approximately 3 mW at a 2 GHz frequency.

The authors in [13] presented a circularly polarized rectenna based on a leaky wave antenna; the antenna is printed on Rogers Ro4003C with dimensions of $297 \times 70 \times 1.52\,\text{mm}^3$, an operating bandwidth from 2 to 8 GHz, and a maximum gain of 9.8 dBi. Its rectifier part has an area of $376.5 \times 103.3\,\text{mm}^2$ and provides a maximum power conversion efficiency of 53.8% at 4 GHz. An ultra-wideband rectenna of a conical pyramid as a radiating structure, characterized by a radius of 15 mm and a ground plane width of 23.5 mm printed on a $70 \times 70 \times 1.6\,\text{mm}^3$ FR4 substrate, has been proposed in [14]. It captured energy from 1.5 up to 4.65 GHz and provided conversion efficiency higher than 65%. A compact multiband hybrid fractal antenna is realized in [15] by considering FR4 material of 4.4 dielectric constant and total ndimensions of $36 \times 36 \times 1.6\,\text{mm}^3$. It covers two important bands at 1.84 GHz (downlink GSM 1800), 5.55 GHz (lower WLAN) and provides VSWR ≤ 2 and $S_{11} \leq -10$ dB with considerable gain values. An energy harvesting antenna of total dimensions $(0.6\lambda_0 \times 0.4\lambda_0 \times 0.0128\lambda_0)\,\text{mm}^3$ is presented in [16], for 2.4 GHz Wi-Fi requests. It covers a measured wide bandwidth from 2.24 up to 3.05 GHz; besides, two resonances at 2.4 and 2.8 GHz with a peak gain, respectively, of 2.4 dB and 4.7 dB have been achieved with almost 95.2% radiation efficiency.

In contrast, [17] identifies a slotted Koch snowflake fractal-patch antenna of $102 \times 102 \times 1.6\,\text{mm}^3$ dimensions, besides a half-wave rectifier circuit with a manufactured pi matching network. It provides an operation at an almost 2 GHz frequency, measuring S_{11} lower than -10 dB and 51.7% power conversion efficiency at 2 dBm for 2.11 GHz frequency applications. A monopole microstrip antenna with dimensions of $140 \times 60 \times 1.6\,\text{mm}^3$ for GSM/GPRS, WiMAX, and WLAN applications is presented in [18]. It is fabricated on an FR4 substrate material and operates from 1 up to 8 GHz with a maximum gain of 3 dBi and efficiency greater than 80% at 2.45 GHz. Its integrated rectenna system has 50% power conversion efficiency with a maximum power density of 25 μW at -20 dBm input power. In [19], a 2D rectenna is made up of polylactic acid polymer (PLA) substrate with a fused deposition modelling (FDM) to obtain 3D shaping for (2.45 GHz) Wi-Fi applications. The dimensions and the dielectric constant of the fab-

TABLE 1. Literature review summary with different types of rectenna designs.

Ref	Year	Author	Antenna type	Rectifier element	Remarks
[1]	2018	Qasim Awais	A slotted planar antenna	HSMS-2850 diode	Single-stage Cockcroft-Walton rectifier with L-shaped impedance-matching network, with low conversion efficiency.
[8]	2024	Neeta Singh	Low-profile flexible antenna	HSMS-282E in a SOT 323 package	Low power conversion efficiency.
[9]	2021	Omaima Benkhadda	Octagonal radiator with Vicsek fractal slots and a partial ground plane	———	Not supported with rectifier circuit.
[10]	2021	Rashmi Pandey	Rectangular patch dual circular radiating elements	HSMS 2813	Narrow B.W for antenna and rectenna design.
[11]	2022	Amit Baran Dey	CPW fed antenna with slot	HSMS-2850 diode-based hybrid voltage Tripler circuit	Coplanar waveguide fed rectenna system with low power conversion efficiency.
[12]	2023	Melad M. Olaimat	Triangular patch antenna (TPA), consists of a metallic radiating patch backed by a ground plane	HSMS-2860 Schottky diode	11 segments of T.L. printed on the top of a thick dielectric substrate to achieve higher power conversion.
[13]	2026	Nesma Mohamed	Circularly polarized leaky wave rectenna (CPLWA)	SMS7630-079LF Schottky diode	High efficiency antenna is designed. However, low power conversion efficiency with large size antenna design.
[14]	2024	Shailendra Singh Ojha	Compact conical antenna	HSMS 2850 Schottky diode	Dual ultra-wideband rectenna, However, low power conversion efficiency is achieved.
[15]	2024	Manpreet Kaur	Hybrid fractal antenna	———	The antenna is designed for RF energy harvesting. However, not supported with rectifier circuit.
[16]	2021	Akhilesh Kumar	MIMO antenna	P21XXCSR board	The antenna is supported by power management energy harvesting board. However, low power conversion efficiency is achieved.
[17]	2025	Ming Wei Sing	Slotted Koch snowflake fractal patch	SMS7630-040 LF	Low power conversion efficiency is achieved with a large size antenna design.
[18]	2025	Dalia N. Elshaekh	Monopole antenna	SMS 7630 Schottky diode	Low power conversion efficiency is achieved with a large size antenna design.
[19]	2023	Pangsui Usifu Linge	Patch antenna printed on Polylactic Acid Polymer substrate	HSMS 2850	The obtained power conversion efficiency somewhat lower $< 30\%$.
[20]	2024	Amira A. Khedr	Dual-port (2×1) UWB-MIMO antenna	———-	The antenna activates small hand-held devices with the required energies, however lower gain obtained at 2.45 GHz.
[21]	2023	Seong-Jin Kim	A Planar stepped bow-tie antenna	SMS7630-005LF	Lower gain value obtained at 2.45 GHz.

ricated antenna are $80 \times 70 \times 1.5\,\text{mm}^3$ and 2.9, respectively. It provides a measured S_{11} lower than -10 dB and a total gain of 7.5 dBi. Dual-port UWB-MIMO four A-shaped slots fabricated on Rogers RT 5880 with dimensions $39 \times 30 \times 0.8\,\text{mm}^3$ is presented in [20]. The antenna activates small hand-held devices, such as smartwatches, phones, and tablets with required energies besides measured S_{11} and gain values, respectively, of -10 and 2 dBi at 2.45 GHz. A planar stepped bow-tie antenna reported in [21], with dimensions of $68 \times 107 \times 1.6\,\text{mm}^3$ and operating in a frequency band ranging from 0.85 to 3.66 GHz, achieves gain values ranging from 0.96 to 4.74 dBi. It includes a power management unit for RF energy harvesting for IOT systems, which provides a maximum power energy conversion value of 75.6%.

Table 1 summarizes the above types of rectenna designs by providing a brief comparison in terms of the antenna and the rectifier element used.

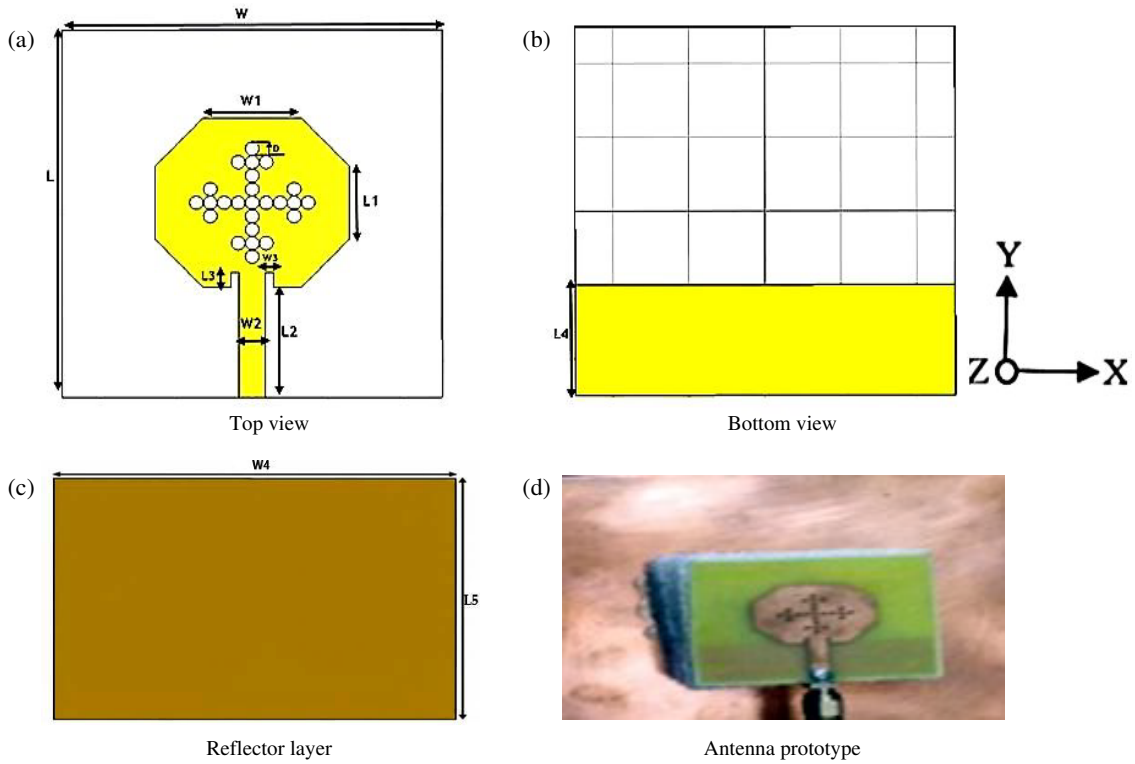

FIGURE 1. Proposed antenna basic structure.

The recent literature still lacks coverage of issues such as simple planar antenna structure for optimizing gain and enhancing energy conversion efficiency. To enhance different wireless applications, this study aims to close this gap by creating an optimal planar structure for wireless communication systems and targeting high conversion efficiency under realistic operations, particularly for wireless energy harvesting applications at the ISM band.

In this literature, an octagonal patch antenna loaded with circular slots backed with both DGS and a copper reflector layer has been designed to provide the following novelties:

1- The proposed antenna fulfills a measured impedance bandwidth of 4.9 GHz from 2.1 up to 7 GHz with a maximum peak gain of 8 dBi, providing operations in various industrial applications (WLAN, Wi-Max, etc.) compared to current designs.

2- Highlight the research development of a complete rectenna design with efficient integration of its individual modules to optimize the overall planned system operation under realistic and lower input power situations.

3- The proposed system introduces a simple design, cost-effective, and harvesting capability of capturing the incident energy at 2.45 GHz without the need for multiple-input multiple-output (MIMO) ports or frequency selective (FSS) layers.

4- It provides three crucial resonances at 2.45, 3.8, and 5.6 GHz with high gain values resulting from the integration of an octagon-shaped radiator patch, circular slots supported by a defected ground structure (DGS), and a copper reflected layer.

5- Significantly, the power conversion efficiency exceeds 85% at 2.45 GHz frequency.

The detailed study of the proposed antenna in terms of design evolution, antenna geometry, results and discussion, RF power harvesting, and the conclusion is presented in the foregoing sections.

Section 2 describes the antenna's design and working principles. Section 3 offers the simulation results of the planner structures. Section 4 presents fabrication and tests of the proposed antenna. Section 5 demonstrates the rectifier part of the rectenna. Finally, Section 6 presents the conclusion.

2. ANTENNA SYSTEM DESIGN

The structure of the proposed antenna is presented in Fig. 1. It is constructed from an octagonal radiator loaded with circular fractal slots embedded on a 1.6 mm-thick FR4 dielectric substrate of a 4.4 relative permittivity and 0.02 loss tangents. The antenna dimensions are $47 \times 47 \times 1.6\,\text{mm}^3$ in addition to a DGS of $14.6 \times 47 \times 1.6\,\text{mm}^3$ as plotted in Figs. 1(a) and (b). It is mainly engineered to provide the operational requests at different resonances within the desired bandwidth. The designed structure is then excited through a transmission feed line (T.L.) of width $W2$, length $L2$ besides an inset feed of length $L3$ and gap $W3$.

Firstly, circular slots have been designed by calculating their diameters regarding the equations that are described in [22, 23]. A rectangular microstrip antenna of length L and width W was

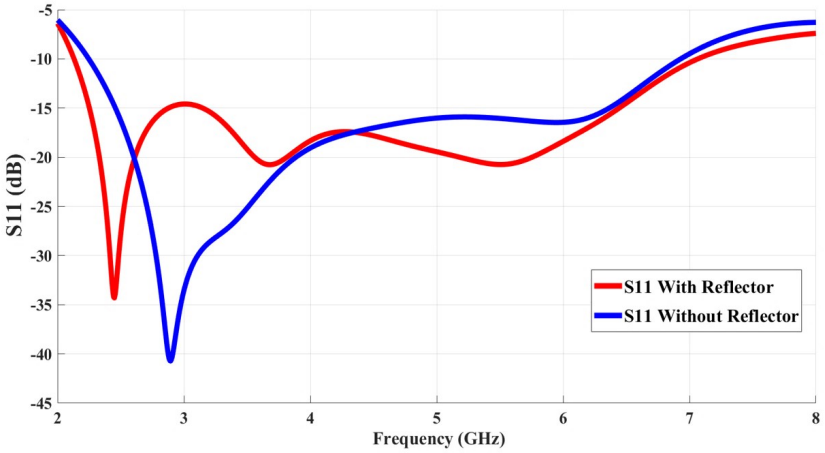

FIGURE 2. S_{11} simulated results of the proposed antenna with and without reflector.

TABLE 2. Proposed antenna dimensions (mm).

Proposed Antenna Variables Dimensions				Patch Antenna overall Dimensions		
Variables	**Optimized dimensions**	**Variables**	**Optimized dimensions**	**Total length**	**Total width**	**Substrate thickness h**
W	47	L	47	47	47	1.6
$W1$	13	$L1$	10			
$W2$	3.5	$L2$	15			
$W3$	2.2	$L3$	1.2			
$W4$	100	$L4$	14.6			
D	1.4	$L5$	100			

taken as a simple reference microstrip patch antenna. Then, the dimensions of the octagon-shaped radiators were determined using the T.L. theories according to the formulas presented in [24]. The initial values for the antenna dimensions have been established along with the parametrically studied through the CSTMWS simulators to match the considered antenna parameters within the operating bandwidth. The antenna's optimum design parameter values are then presented in Table 1. The printed antenna geometry has three main parts as depicted in Fig. 1. The top side view of the engineered antenna, as shown in Fig. 1(a), has a dimension of $(47 \times 47 \times 1.6)\,\text{mm}^3$. The circular slots are taking place in the center of the octagonal radiators to improve the antenna structure's operating performance and achieve 2.45 GHz resonant frequency. The DGS layer of dimensions $(14.6 \times 47 \times 1.6)\,\text{mm}^3$ is then plotted in Fig. 1(b), and finally, a copper reflected layer at a distance of 26 mm from the radiator patch is taking place with a dimension of $(100 \times 100 \times 1)\,\text{mm}^3$ as depicted in Fig. 1(c). To avoid the higher-order modes of operation and obtain the 50 Ω microstrip line matching impedance, the metallic T.L. cut-off frequency will be calculated with an accurate selection of the line feed substrate's length, keeping the minimum loss in the microstrip line feed at $(L2 + L3)$ mm. As the reflection of the arriving wave is diminished according to the impedance matching methodology, a microstrip feed line with the optimized dimensions $W2$ and $(L2 + L3)$ mm is loaded on a similar substrate for appropriate excitation. Therefore, an octagonal patch of circular slots backed with DGS and a metallic reflector layer is designed with a planar 50 Ω T.L. The selected substrate parameters realize up to 7 GHz operating frequencies without the higher-order modes of operation as shown in Fig. 1(d) [22, 24].

3. SIMULATIONS RESULTS

Our aim in this study is to utilize an octagonal microstrip patch, circular slots, backed DGS, and a copper reflector layer to achieve the required resonant frequencies within the entire bandwidth. Firstly, the physical parameter for the octagonal patch loaded with circular slots is optimized through the parametric study for obtaining their dimensions nearly equal to $\lambda_g/2$. The influence of the DGS rectangular-shaped patch dimensions provides many features, such as increasing the impedance bandwidth and suppressing the surface wave using the antenna parametric study. Then, a copper reflector layer is responsible for shifting the frequency resonances and obtaining high gain values over all the operating bandwidth. Lastly, testing the difference in antenna characteristics, due to various parameters stated in Table 2, has taken place by the CST simulator. It is considered through the input reflection coefficient (S_{11}) that relates the planned antenna absorption power measured at the feed input over the total power [2]. The

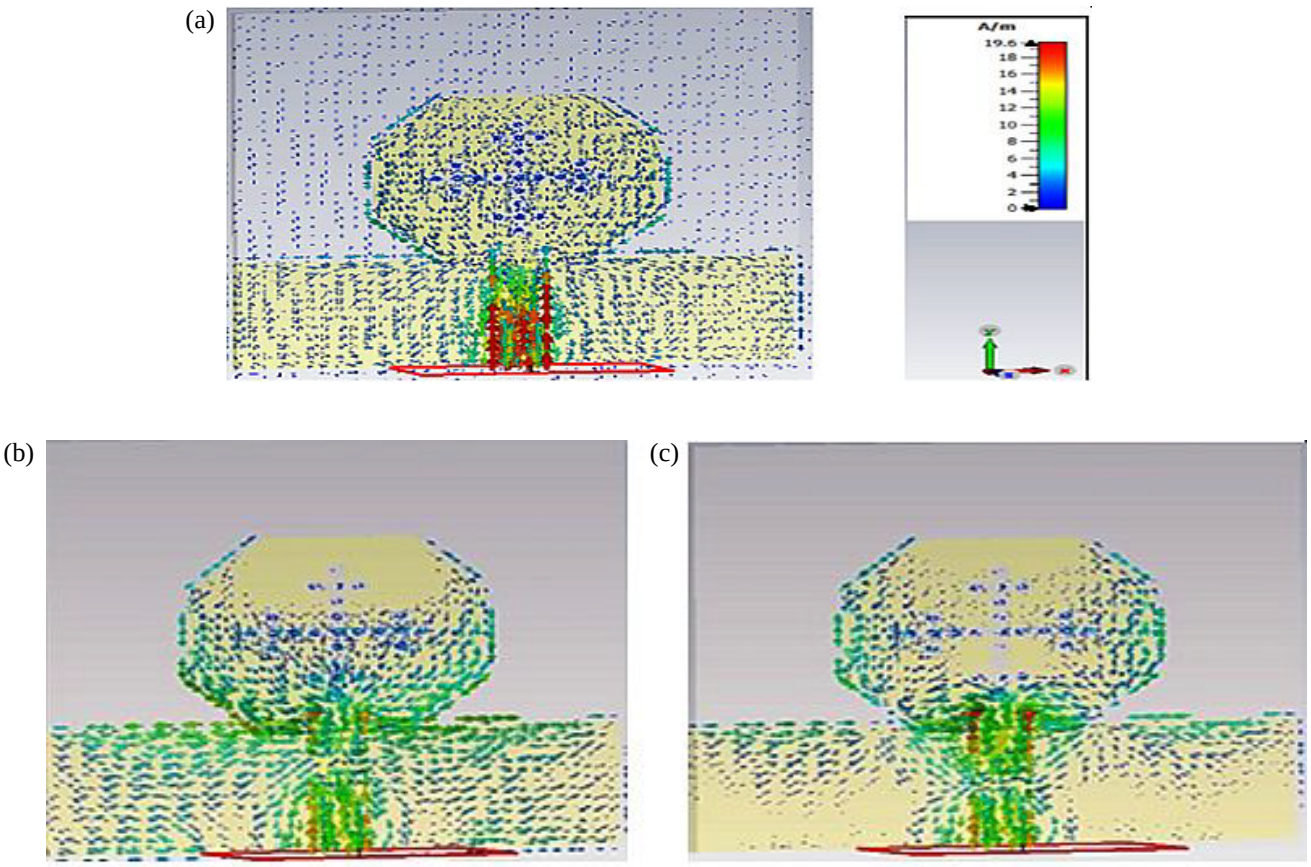

FIGURE 3. Surface current distribution for the proposed design at different frequencies. (a) @ 2.45 GHz, (b) @ 3.88 GHz, (c) @ 5.6 GHz.

CST (S_{11}) results over the entire bandwidth and the three obtained resonances are characterized in Fig. 2. A lower (S_{11}) power of nearly -40 dB has been obtained from the CST simulator at 2.9 GHz without using a reflector layer. However, in the case of using the reflector layer, the S_{11} value became -35 dB with a resonant frequency centered at 2.45 GHz, which is suitable for Industrial, Scientific, and Medical (ISM) band applications driven by the best matching impedance. Similarly, 3.8 and 5.6 GHz resonances having (S_{11}) values $<$ -20 dB indicate a lower matching impedance at these values. It should be noted that the antenna fulfills the UWB characteristics from 2.1 : 7 GHz with tri-resonances between 2.1 : 2.9, 3.5 : 3.85 and 5.2 : 6.5 GHz covering ISM (2.45 GHz), Wi-Max (2.5/3.5/5.5) GHz and WLAN (2.4/5.2/5.8) GHz bands [25].

Accordingly, the octagonal patch with the circularly loaded slots, besides the rectangular DGS, provides operation in triple-frequency resonances. While the reflector layer, which is 26 mm distance apart from the octagonal patch, achieves the shifting in the operating frequency of the first resonant as shown in Fig. 2.

3.1. Surface Current Distribution on the Proposed Antenna

The CST simulator has also provided an outline of the surface current density distribution for the proposed planar structure at the specified resonant frequencies. Consequently, the surface current density at the patch radiators loaded with circular slots at some designated frequencies is plotted in Fig. 3, where the blue and red colors characterize the lowest and strongest surface current distribution areas individually. The mechanism of the EM radiations mainly results from the distributions of the current densities within the edges of the radiator patch, filled by the circular slots and around the surface of the feed line. Therefore, at a frequency of 2.45 GHz presented in Fig. 3(a), the surface current was mainly distributed around the edges of the antenna feed line and also, to a lower degree (yellow color), on the inside of the radiator patch except for the loaded inner circular slots, which have gained the lowest current densities (blue colors). It can be noted that at 3.8 GHz, the strongest surface current density is concentrated at the lowest area of the radiating patch antenna that intersected with the feed line as in Fig. 3(b), besides at the beginning of the feed line with a reasonable coupling between the antenna patch and the feed line. At 6 GHz, the critical influence is due to the constructive coupling between the antenna patch and the feed line, which is depicted in Fig. 3(c). As a result of this strong coupling, much energy is transferred to different planar structure places.

Consequently, the distribution of the intensive surface currents on the edges of the inner slot (inserted at the DGS rectangular patch) is more resourceful than the feed line. Nevertheless, the shift around the frequency resonances is due to the effect of DGS underneath the various patches, which achieve

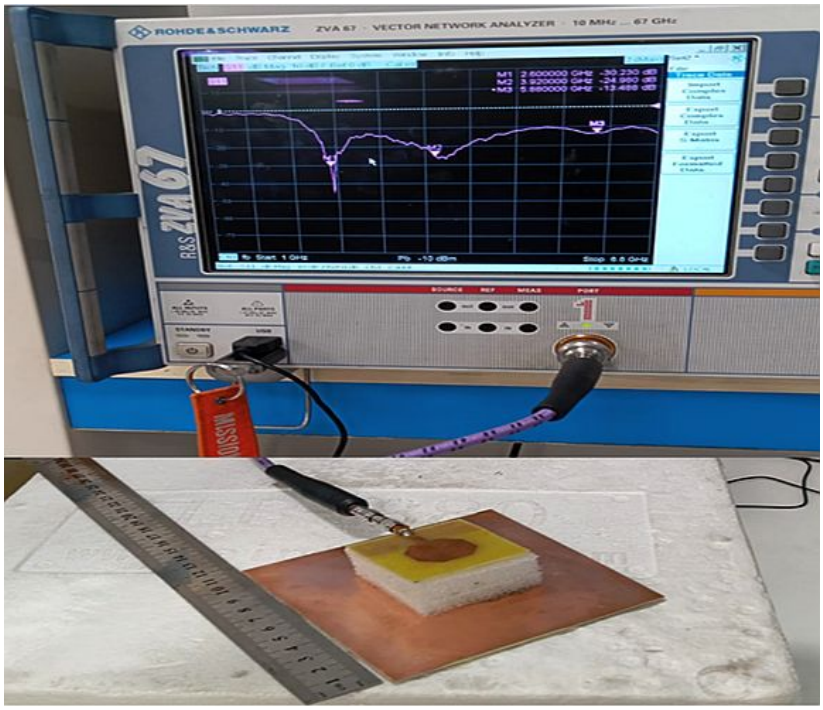

FIGURE 4. Test bench used for measuring the antenna input reflection coefficient (S_{11}) values by a VNA.

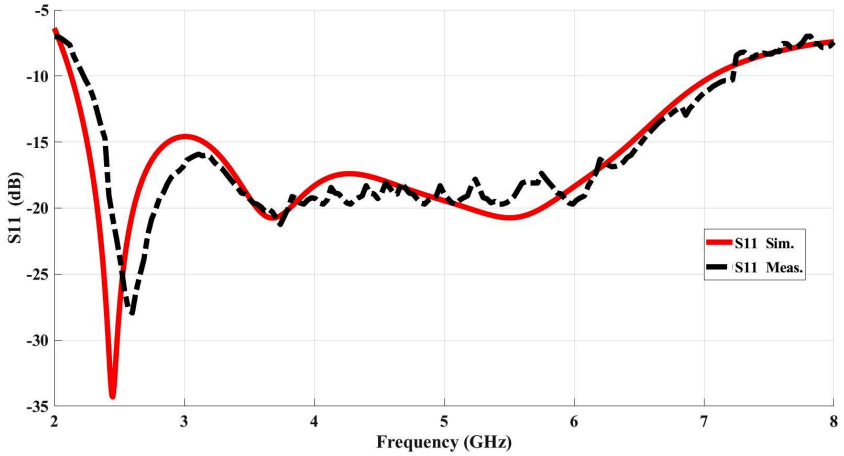

FIGURE 5. Measuring vs. simulated antenna input reflection coefficient (S_{11}) values.

a wider triple-band performance based on optimizing the DGS to increase the operating bandwidth around the resonating frequencies [26, 27].

4. FABRICATION AND TESTS

Due to the foregoing implicit analysis, attractive surface current density features, obtained resonances, and the operating bandwidth, a direct perception of the designed antenna's performance is realized. The engineering process has been executed to validate the antenna's simulation results and its physical characteristics. The input reflection coefficient (S_{11}) parameter of the manufactured prototype was tested by the 50 Ω port of the ZVA 67 Rohde & Schwarz vector network analyzer (VNA). The S_{11} measurement setup is shown in Fig. 4, where the VNA port 1 is directly connected via a coaxial cable to the antenna's end terminal as described in [29]. Fig. 5 characterizes the measured antenna reflection coefficients over the frequency operating bandwidth. The relationship between the measured and simulated (S_{11}) results is evaluated for the dissimilarities between them. After the manufacture and measurements of the antenna prototype, the (S_{11}) physical characteristics at the allocated frequency bandwidth were noticeably achieved. Basically, the frequency bands are centered at three different frequencies (2.45, 3.8, and 5.6) GHz; besides, it extends from 2.1 up to 7 GHz. With regard to the comparison between the simulated results and the measured ones, as shown in Fig. 5, the results indicated good consistency between the

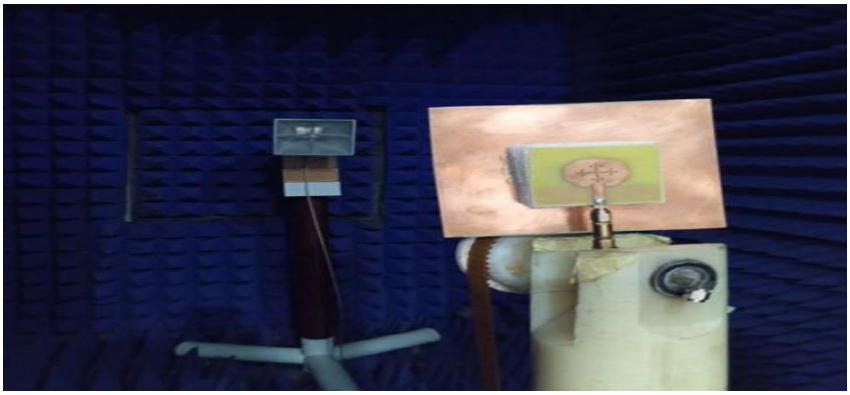

FIGURE 6. Anechoic chamber measurements setup for the manufactured antenna.

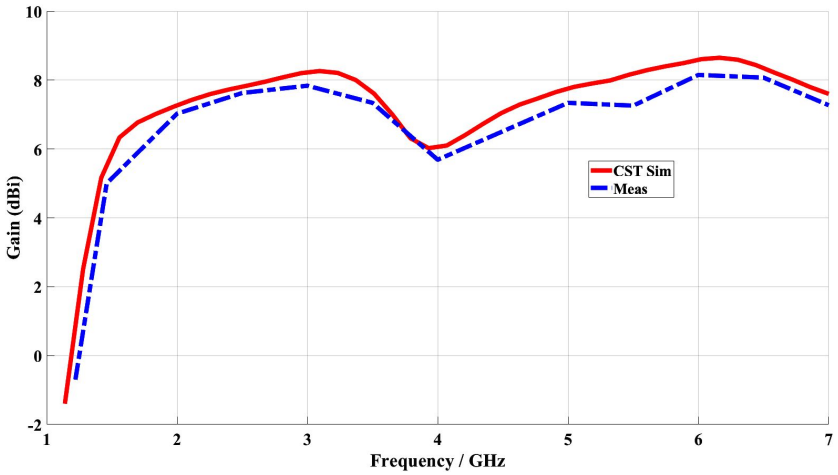

FIGURE 7. Simulated vs measured 2-D gain for the designed antenna.

measurements and CST simulation results within the operating frequency range. Also, wider impedance bandwidths within the allocated resonances are attained by the existence of the DGS layer [22, 28].

Additional examination was done on the fabricated antenna by testing the 2-D, 3-D radiation characteristics at the resonant frequencies and calculating the antenna gain values over the operating bandwidth. The 2-D radiation pattern measurements are done in an anechoic chamber as depicted in Fig. 6. Herein, a double-ridged horn antenna is utilized as a transmitting end to support measuring the antenna prototype radiation pattern on both E and H planes. The receiving terminal for the manufactured sample is fastened at 65 cm apart from the transmitting end to fulfill the far-field requirements. The line-of-sight direction is then taken in between the transmitting and receiving ends, and antenna radiation is inspected by rotating it over the elevation and horizontal planes. The gain is also taken by measuring the insertion loss (S_{21}) of the fabricated antenna through connecting it to the ZVA67 Network Analyzer's port 1 and the reference (horn antenna) to port 2. Table 3 exhibits the tested and normalized simulated radiation patterns at the obtained resonant frequencies in both E (Phi $=$ 0°) and H (Phi $=$ 90°) planes. Generally, the distribution effect takes place at the higher frequencies as a result of the higher order-mode excitations [1]. It should be noted that from Table 3(a), the antenna radiation patterns have nearly bidirectional behavior in both YZ and XZ planes, which are suitable for the RF energy harvesting requests at 2.45 GHz (WLAN) frequency. The same behavior has almost been obtained in the E and H-planes at 3.88 GHz (second band), as tabulated in Table 3(b), while at 5.6 GHz (third band) in Table 3(c), the antenna patterns display a close to bidirectional performance in both E and H planes. Accordingly, broadside directions were achieved in the H-plane in each of the three resonances in both measured and simulated 2-D radiation patterns, as stated in Table 3.

The simulated and measured 2-D gain values of the proposed antenna are shown in Fig. 7, where a maximum gain of almost 8 dBi is achieved at 2.45 GHz. Generally, choosing a high gain is suitable for a known receiver location, and, on the flip side, a lower gain permits the collection of the RF signals from different directions. It is noted that the antenna prototype maintains the same characteristics over the overall operating bandwidth with an average measured high gain value of almost 8 dBi within the entire operating bandwidth, as shown in Fig. 7. The fabricated antenna configuration has a slight variation in the gain magnitude at the 3.88 GHz frequency. This substantial

TABLE 3. 2D/3D radiation patterns of the antenna on the $E(xz)$ and $H(yz)$ planes: simulated (- - - - Dashed line) and measured (—— Solid line) at three different frequencies (a) 2.45, (b) 3.8, (c) 5.88 GHz.

	(xz plane) Phi=0	*3D Radiation*	*(yz plane) Phi=90*	*3D Radiation*
(a) **2.45**	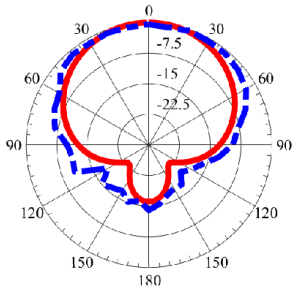	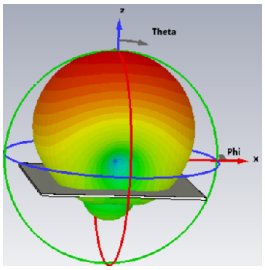	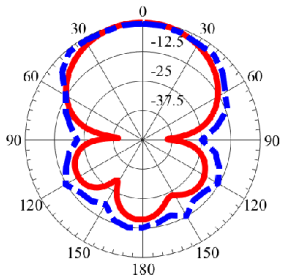	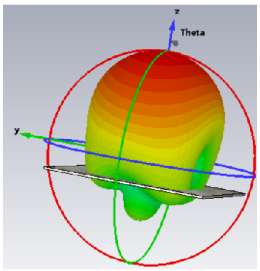
(b) **3.8**	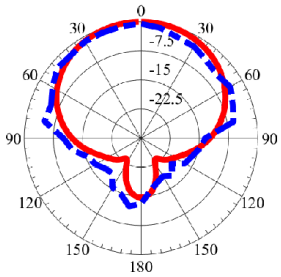	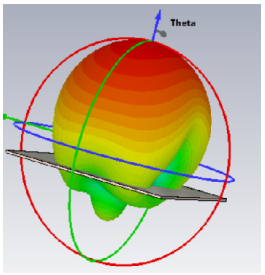	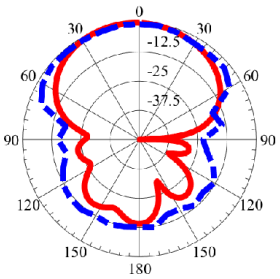	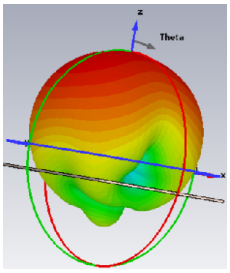
(c) **5.88**	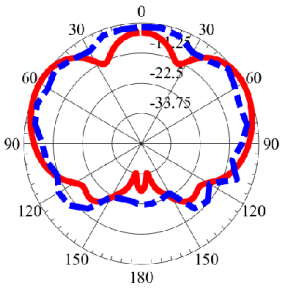	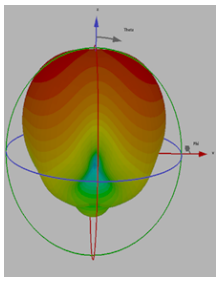	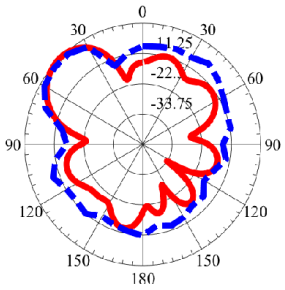	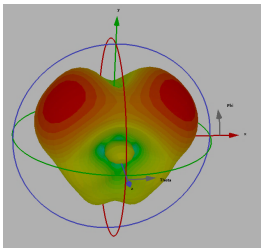

variation is due to several antenna elements creating dissimilar edge impedances. Subsequently, the highest gain is provided with better impedance matching, while the lowest gain is produced by lower impedance matching.

5. RECTIFIER CIRCUIT MODELING FOR THE PROPOSED DESIGN

Normally, series or parallel RLC circuits are utilized to create the equivalent circuit model for the proposed design. The microstrip antenna achieves a band-pass filter performance where the undesirable frequencies are weakened by the proposed antenna design, except those placed in the wanted range. Accordingly, the antenna's S_{11} values of the resonant frequencies have been modeled by using parallel, series, or both series and parallel resonant circuits by means of the Advanced System (ADS) toolbox. The association of the desired resonant frequencies within their demanded bandwidth through the lumped components is completely described in [22].

Moreover, the RF energy harvesting rectifier circuit typically comprises different sections besides the proposed antenna model, such as the impedance matching network, voltage multiplier, DC filter, and load. A matching network is crucial for transferring maximum receiving antenna power to the rectifier circuit and harvesting of the obtainable RF energy at low power density values, typically from -50 dBm up to -20 dBm. Also, obtaining the desired RF system output power depends on the distance between the RF source and the rectifying circuit, besides the efficiency of this rectifier circuit. The voltage level of the RF signal ranges from 0.1 to 1 V which cannot operate many electronic devices. Consequently, a Cockcroft-Walton voltage multiplier with a single-stage circuit is used in our plan besides fast switching of two high-frequency diodes (HSMS-2850) with a low forward biasing of 0.15 V to keep up with very low RF input power applications.

The inductor and capacitor values for the impedance matching network are optimized by the ADS design tuning utility, and multiplier capacitor parameters are calculated from the fol-

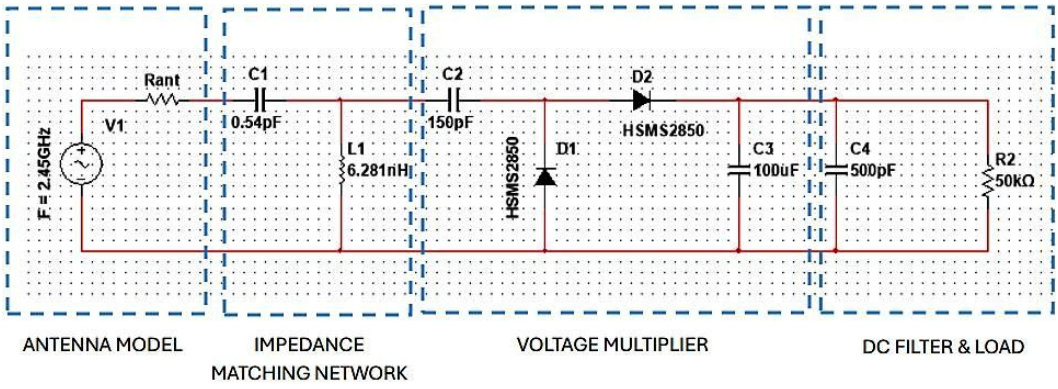

FIGURE 8. Proposed antenna RF energy harvesting rectifying circuit network.

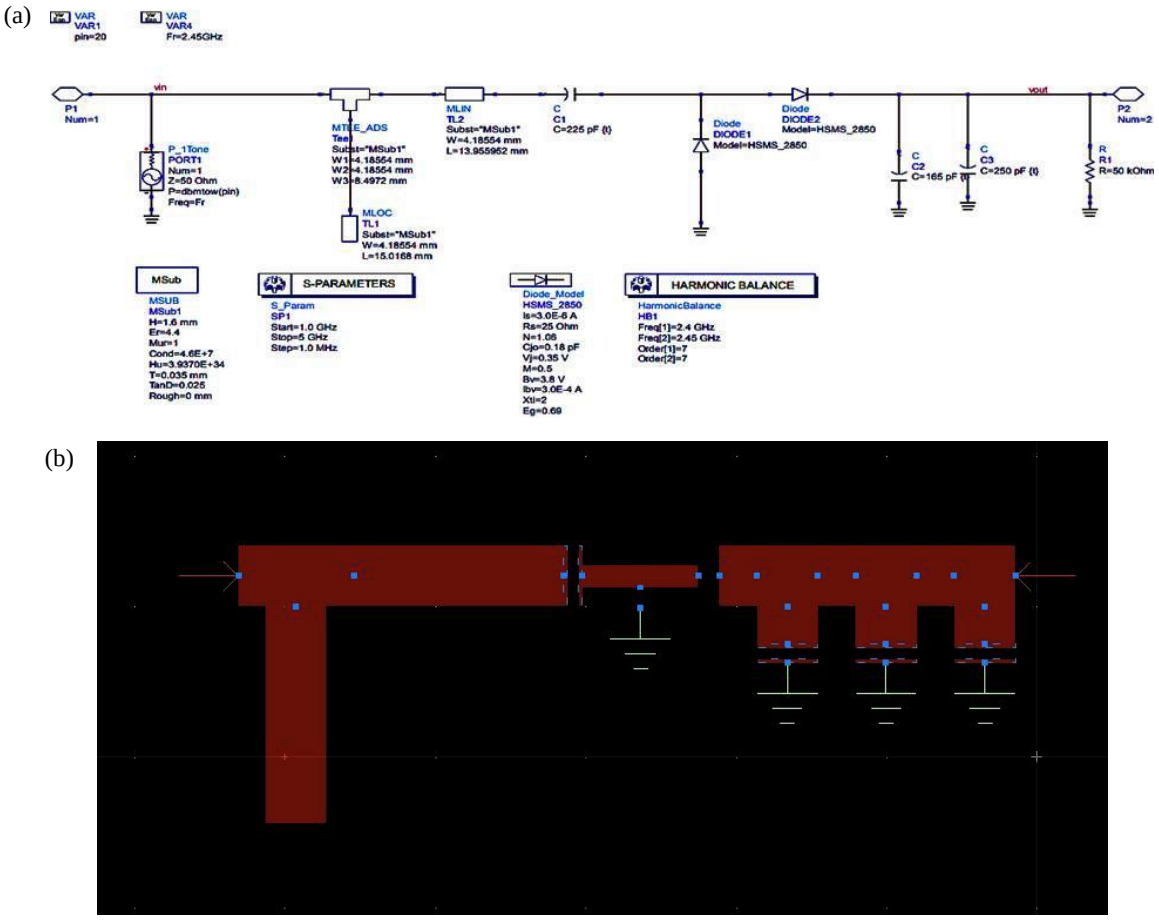

FIGURE 9. Advance Design System (ADS) schematic of the rectifier equivalent circuit model. (a) Rectifier circuit schematic diagram. (b) Layout.

lowing equation [1].

$$C = \frac{Q}{V} = I\frac{dt}{dV} \quad \& \quad V = L\frac{di}{dt} \tag{1}$$

where C, L, I, $\frac{dt}{dV}$, and $\frac{di}{dt}$, respectively, represent the desired capacitance, inductance, current on each branch, the rate of change of the voltage w.r.t frequency, and the rate of change of the current. The network topology used for the desired rectifier circuit is plotted in Fig. 8, along with its impedance matching network, voltage multiplier, and filter load section. Herein, the received RF AC signals are converted to DC by the full-wave rectifier circuit section. The diodes $D1$ and $D2$ are operated consecutively at the negative and positive cycles to store the energy in the capacitor $C1$.

Thus, the voltage across $C1$ and then the output voltage are calculated by the following relations [1].

$$V_{C1} = V1 - V_{thD1}, \quad V_{OUT} = 2V1 - V_{thD1} - V_{thD2} \tag{2}$$

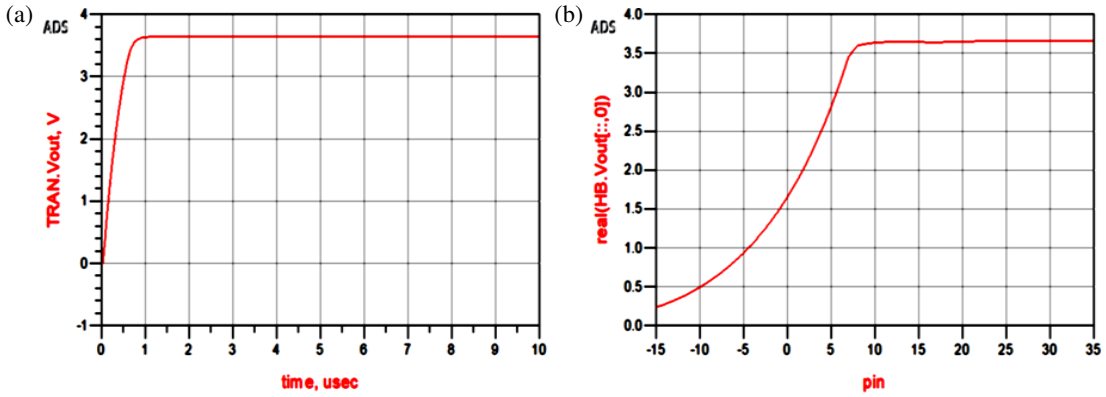

FIGURE 10. Simulated (a) transient V_{out} response, (b) V_{out} at different input RF power levels.

where $V1$ is the AC input voltage; V_{thD1}, V_{thD2} and V_{Out} are the diodes thresholds and rectifier DC output voltages, respectively.

The T.L. model and simulation variables for the proposed antenna, followed by the RF harvesting rectifier circuit, are simulated using the Advance Design System (ADS) simulator, accompanied by its layout as depicted in Fig. 9. As the FR4 substrate with a thickness of 1.6 mm is selected for the rectenna fabrication, the input impedance of the voltage multiplier is then calculated to be $15.75 - j11.6\,\Omega$ [1]. This value relies on many factors, such as the antenna resonant frequency, overall circuit input power levels, and its load conditions. In the ultimate recent rectenna, multiple impedance-matching networks per rectifier circuit are usually used in one design to achieve multiband characteristics. A big challenge is to obtain wideband width performance for the rectenna at the operating resonant frequency [29, 30]. Our designed rectifier has a reasonable bandwidth ranging from 2.1 : 2.9 GHz which is more than the stated values in [1, 19, 31].

The two Schottky diodes (HSMS2850) were selected for their good RF-to-DC efficiency at very low input powers and for single-band rectification while the double transmission lines (TL.1, TL.2) conduct the EM waves and carry the electrical energy from the input source with minimal losses. The values of capacitors at different harvesting rectifier circuit sections along with the load resistance are tabulated in Table 4. Generally, ADS simulator functions comprise different simulation technologies, such as circuit, system, and EM radiation that are used for various analysis tasks like harmonic balance (HB), DC and S-parameter harmonic balance, and high-frequency EM analysis.

The simulated transient output voltage (V_{out}) response of the rectifier circuit and the obtained V_{out} at different input RF power levels are plotted in Fig. 10.

TABLE 4. Lumped element values in the designed rectenna.

Resistors (ohm)	Capacitance (PF)
$R1 = 50000$	$C1 = 150$
	$C2 = 150$
	$C3 = 500$

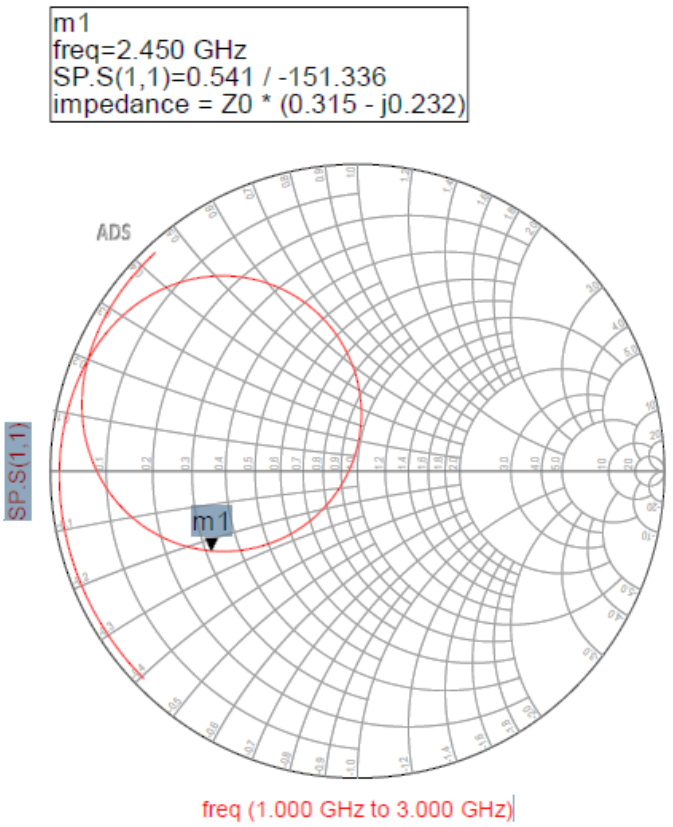

FIGURE 11. Smith chart representation of impedance matching characteristics.

The transient response in Fig. 10(a) indicates that the initial output of a rectenna system has a very quick rise time, subjected to an abrupt input before reaching its steady-state response. This is done by using two fast-switching high-frequency (HSMS-2850) diodes with a low forward biasing (0.15) V. Additionally, keeping up with the very low RF input power applications can be supported by the selected (HSMS-2850) diodes. The simulated V_{out} versus the RF input power at 50 kΩ load resistance is shown in Fig. 10(b).

As the optimum load resistance typically varies with changing the frequency and input power values, we optimize the load resistor in ADS under the low input power constraint of

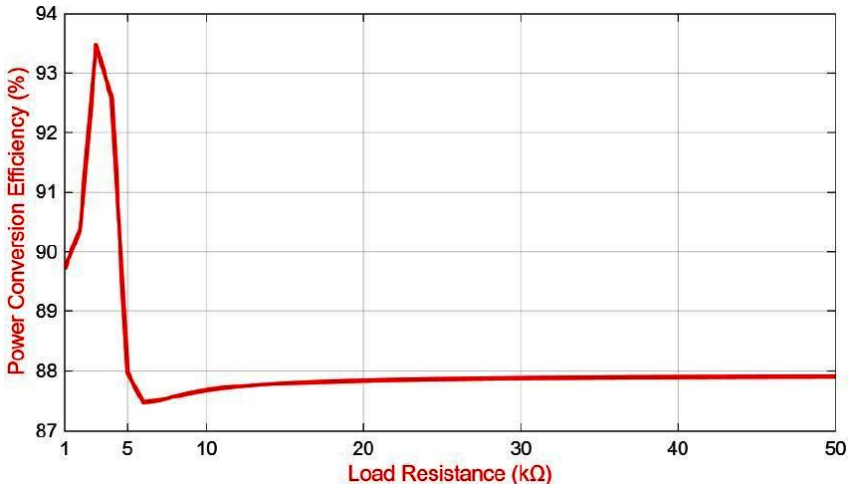

FIGURE 12. Rectenna simulated power conversion efficiency at 2.45 GHz vs. different load resistance values.

FIGURE 13. Rectenna simulated power conversion efficiency at 2.45 GHz vs. different input power values.

-15 dBm to maximize the obtained V_{out} around the 2.45 GHz frequency and the optimum load resistor of 50 kΩ. The simulated V_{out} value of almost 3 V at 5 dBm and nearly 3.5 V for RF input power values from 7 up to 35 dBm has been achieved, which indicates that the designed rectifier circuit has good operational performance in the required bandwidth. Finally, the Smith chart representations of the impedance matching characteristic values at different input power levels of 20 dBm, 10 dBm, and 5 dBm are plotted in Fig. 11. An outstanding impedance matching has been obtained at 2.45 GHz, covering the WLAN's different applications. Moreover, the rectenna also has good matching characteristics from 2.1 GHz to 3 GHz frequencies. The capacitive and inductive components of the impedance deteriorate the matching behaviors outside of this range. The impedance matching value is then equal to $Zo*(0.315-j0.232)\,\Omega$, where the characteristic impedance $Zo = 50\,\Omega$.

The power conversion efficiency at 2.45 GHz for different load resistance and input power (P_{in}) values is then simulated throughout the ADS tool as described thoroughly in [32]. Therefore, the simulated power conversion efficiency at 2.45 GHz for different load resistance and input power (P_{in}) values is plotted in Figs. 12 and 13, respectively. Fig. 12 shows the simulated power conversion efficiency at 2.45 GHz for different load resistance values. The maximum power conversion efficiency versus different load resistance values is obtained within the range from 1 to 50 KΩ. It should be noted that the proposed rectenna design has rising and falling responses in the range from 1 to 5 kΩ load resistance before giving a stable response in the rest of the chosen range. The value of the maximum power conversion efficiency is $> 90\%$ at 2.5 KΩ and it is almost 88% within the range from 6 to 50 KΩ. Among these values, the optimized load resistance has been selected as 50 KΩ.

TABLE 5. A comparison between the proposed antenna and other published papers.

Ref.	Antenna Size (mm^3)	Substrate type/ Relative permittivity	Antenna/ Rectifier B.W (GHz)	Antenna Gain (dBi)	No of (T.L.)/ material	Conversion efficiency/Input power level	Applications
[1]	$30 \times 18 \times 1.6$	FR4 $\varepsilon_r = 4.4$	(2.37–2.52)/ (2.37–2.52)	5.6	2/FR4	68% at 5 dBm for 4.2 GHz	WLAN/Wi-Fi (2.45 GHz)
[8]	$25.2 \times 21.5 \times 0.053$	Low profile bio-compatible polyimide substrate $\varepsilon_r = 3.4$	(1.8–3.4)/ (1.8 : 3.4)	3.2	1/Low profile bio-compatible polyimide substrate	78.2% at -5 dBm for 4.2 GHz	Smartwatchs & Wristband at WLAN/Wi-Fi (2.45 GHz)
[9]	$50 \times 50 \times 1.6$	FR4 $\varepsilon_r = 4.4$	(2.48–6.7)/NA	2.78 at 3.6 GHz & 5.32 at 5.3 GHz	ND	ND	WLAN/Wi-Max IoT sensors
[11]	$40 \times 35 \times 1.6$	FR4 $\varepsilon_r = 4.4$	(1.7–3)/ (2.36–2.45)	4.12	1/FR4	66.7% at 5 dBm for 42 GHz	Bluetooth/WLAN
[12]	Three layers; 1- $69.3 \times 69.3 \times 1.27$ 2- $69.3 \times 69.3 \times 11.71$ 3- $69.3 \times 69.3 \times 1.52$	1- $\varepsilon_r = 2$ 2- $\varepsilon_r = 1$ 3- $\varepsilon_r = 3.66$	(1.75 : 2.26)/ (1.75 : 2.26)	ND	11/Rogers RO (3006)	ND	Microwave Communications at this band
[13]	$297 \times 70 \times 1.52$	Rogers Ro4003C	(2–8)/ (4.2)	9 on average	4/RO4003C	53.8% at 2 dBm for 4.2 GHz	Wi-Fi 2.4, WLAN, WiMAX and the 5G mid-bands
[17]	$102 \times 102 \times 1.6$	FR4 $\varepsilon_r = 4.4$	(2.07–3.9)/ (1.8–2.47)	ND	2/FR4	51.7% at 2 dBm for 2.11 GHz	Real-world IoT applications
[19]	$70 \times 80 \times 1.52$	polylactic Acid polymer $\varepsilon_r = 2.9$	(2.4–2.47)/ (2.4–2.47)	7.5	1/PLA	28.75% at -10 dBm for 2.45 GHz	Wi-Fi
[31]	$34 \times 25 \times 1.6$	FR4 $\varepsilon_r = 4.4$	(2.45 and 5.2)/ (2.45 and 5.2)	ND	2/FR4	75% at 0 dBm for 2.45 GHz	ISM bands
[34]	$56 \times 47 \times 1.57$	Rogers 5880 $\varepsilon_r = 2.2$	(2.42–2.47)/ 2.45	9	ND	ND	(ISM) band 2.45 GHz
This Work	$47 \times 47 \times 1.6$	FR4 $\varepsilon_r = 4.4$	(2.1–7)/ (2.1–2.9)	8 on average	2/FR4	98.4% at -10 dBm, 95.8% at 0 dBm, and 88% at 20 dBm for 2.4 5 GHz	ISM, WLAN/ Wi-Max &lower/upper bands of 5G mobile systems

Generally, the RF to DC total conversion efficiency at different RF input powers of the proposed rectenna can be calculated by the following equation [33]:

$$Power \text{ Conversion Efficiency } \% = \frac{V^2{}_{OUT}}{R_L P_{in}} \times 100 \qquad (3)$$

where P_{in} and R_L are the input power and load resistance respectively.

The simulated power conversion efficiency at 2.45 GHz for different input powers (P_{in}) is plotted in Fig. 13. Herein, the value of the RF input power is considered from -30 to 30 dBm with 3 VDC voltage and 50 kΩ load resistance. It can be shown that the obtained peak efficiency values of the rectenna at 2.45 GHz frequency are 98.4% at -10 dBm, 95.8% at 0 dBm, and 88% at 20 dBm.

In conclusion, Table 5 illustrates a comparison between the planned design and some recently published results. As depicted in Table 5, the fabricated microstrip antenna attained better S_{11}, gain, rectifier bandwidth (BW) values, and radiation characteristics than the formerly designed structures. The proposed UWB antenna exhibited excellent performance within the operational frequency range (2.1 : 7) GHz, including the rectenna usage bandwidth (2.1 : 2.9) GHz. It should be noted that our planned antenna demonstrates broader rectification coverage bandwidth with high gain values.

6. CONCLUSION

In this work, an octagonal microstrip patch antenna loaded with circular slots, backed with DGS and a copper reflector layer to achieve triple-band resonances and UWB coverage, is presented. Its operation comprises a wider bandwidth from 2.1 up to 7 GHz with the possibility of capturing the incident energy at 2.45 GHz. It provides three resonances of reasonable bandwidths at 2.45, 3.8, and 5.6 GHz with high gain values of almost 8 dBi. These frequencies have implications for modern wireless technologies, ISM bands, WLAN-based IoT, WiMAX, and lower/upper bands of 5G mobile system applications. The design stages of the proposed antenna are discussed in detail. The robust couplings among the driven inset feed line, octagonal patch, DGS, and reflector layer give $S_{11} < -10$ dB over the whole operating bandwidth. The Schottky diode of the HSMS-2850 type-based rectifying circuit is considered at the ISM (2.45) GHz frequency band, while the harvesting network is designed to match the 50 Ω antenna input impedance and $15.75 - j11.6\,\Omega$ voltage multiplier input impedance. Compared with advanced designs, it offers a competitive, higher gain with economic and simpler construction. The proposed design provides a real-world, low-cost, and effective solution for powering low-energy wireless, Bluetooth, and IoT sensors from ambient RF sources. In future work, we will focus on antenna optimization in terms of size to fit small IoT devices and optimizing the rectenna design to integrate multiple frequency bands for numerous energy harvesting applications.

REFERENCES

[1] Awais, Q., Y. Jin, H. T. Chattha, M. Jamil, H. Qiang, and B. A. Khawaja, "A compact rectenna system with high conversion efficiency for wireless energy harvesting," *IEEE Access*, Vol. 6, 35 857–35 866, 2018.

[2] Halimi, M. A., T. Khan, D. Surender, N. Nasimuddin, and S. R. Rengarajan, "Dielectric resonator antennas for RF energy-harvesting/wireless power transmission applications: A state-of-the-art review," *IEEE Antennas and Propagation Magazine*, Vol. 66, No. 1, 34–45, 2024.

[3] Onoh, G. N., S. N. Arinze, and N. C. Eli-Chukwu, "Design and development of an ultra-wideband microstrip patch antenna for industrial, scientific and medical band applications," *Advance Journal of Science, Engineering and Technology*, Vol. 4, No. 4, 24–31, 2019.

[4] Balani, W., M. Sarvagya, A. Samasgikar, T. Ali, and P. Kumar, "Design and analysis of super wideband antenna for microwave applications," *Sensors*, Vol. 21, No. 2, 477, 2021.

[5] Benkhadda, O., M. Saih, S. Ahmad, A. J. A. Al-Gburi, Z. Zakaria, K. Chaji, and A. Reha, "A miniaturized tri-wideband sierpinski hexagonal-shaped fractal antenna for wireless communication applications," *Fractal and Fractional*, Vol. 7, No. 2, 115, 2023.

[6] Salleh, S., M. A. Zakariya, and R. M. A. Lee, "A comparison study of rectifier designs for 2.45 GHz EM energy harvesting," *Energy and Power Engineering*, Vol. 13, No. 2, 81–89, 2021.

[7] Shome, P. P., D. Sarkar, T. Khan, N. Shinohara, and Y. M. M. Antar, "From Waves to Watts: Advancements in rectenna arrays for radio-frequency energy harvesting and wireless power transfer," *IEEE Antennas and Propagation Magazine*, Vol. 68, No. 1, 10–24, 2026.

[8] Singh, N., T. Khan, S. Kumar, B. K. Kanaujia, H. C. Choi, K. W. Kim, K. Rambabu, S. R. Rengarajan, and A. A. Kishk, "Ultra-thin flexible rectenna integrated with power management unit for wireless power harvester/charging of smartwatch/wristband," *Scientific Reports*, Vol. 14, No. 1, 7447, 2024.

[9] Benkhadda, O., S. Ahmad, M. Saih, K. Chaji, A. Reha, A. Ghaffar, S. Khan, M. Alibakhshikenari, and E. Limiti, "Compact broadband antenna with vicsek fractal slots for WLAN and WiMAX applications," *Applied Sciences*, Vol. 12, No. 3, 1142, 2022.

[10] Pandey, R., A. K. Shankhwar, and A. Singh, "Design and analysis of rectenna at 2.42 GHz for Wi-Fi energy harvesting," *Progress In Electromagnetics Research C*, Vol. 117, 89–98, 2021.

[11] Dey, A. B., N. Semwal, and W. Arif, "Design of a compact and efficient 2.4 GHz rectenna system for energy harvesting," *Journal of Electromagnetic Waves and Applications*, Vol. 36, No. 13, 1850–1868, 2022.

[12] Olaimat, M. M., V. Nayyeri, and O. M. Ramahi, "Simulation and optimization of rectenna systems," *Scientific Reports*, Vol. 13, No. 1, 17107, 2023.

[13] Mohamed, N., N. A. Eltresy, B. E. Elnaghi, A. Magdy, and E. A. Abdallah, "Wideband circularly polarized leaky wave rectenna," *Scientific Reports*, Vol. 16, No. 1, 4119, 2026.

[14] Ojha, S. S., J. K. Sharma, B. Dhakad, S. Kumar, N. Sharma, A. K. Pandey, S. M. M. Hasnain, S. Kumar, and R. Kumar, "A dual ultra-wideband rectenna with a compact conical antenna for RF energy harvesting from S and C bands," *Results in Engineering*, Vol. 22, 102279, 2024.

[15] Kaur, M., R. Krishan, N. Kaur, and J. S. Sivia, "Invasive weed optimization based compact hybridized fractal antenna design for RF energy harvesting and multifunctional wireless applications," *AEU — International Journal of Electronics and Communications*, Vol. 184, 155428, 2024.

[16] Kumar, A., N. K. Narayaswamy, H. V. Kumar, B. Mishra, S. A. Siddique, and A. K. Dwivedi, "High-isolated WiFi-2.4 GHz/LTE MIMO antenna for RF-energy harvesting applications," *AEU — International Journal of Electronics and Communications*, Vol. 141, 153964, 2021.

[17] Seng, M. W., H. L. Shareef, P. Y. Chan, Y. H. Teh, and C. F. Y. Low, "Experimental investigation on slotted Koch snowflake fractal patch rectenna," *Scientific Reports*, Vol. 15, No. 1, 34601, 2025.

[18] Elshaekh, D. N., H. A. Mohamed, L. Y. A. E. Menam, K. A. Sharshar, and S. I. Kayed, "Multiband printed rectenna for radio frequency energy harvesting (RF-EH)," *Discover Electronics*, Vol. 2, No. 1, 39, 2025.

[19] Linge, P. U., T. Gerges, P. Bevilacqua, J.-M. Duchamp, P. Benech, J. Verdier, P. Lombard, M. Cabrera, P. Tsafack, F. Mieyeville, and B. Allard, "Evaluation of polylactic acid polymer as a substrate in rectenna for ambient radiofrequency energy harvesting," *Journal of Low Power Electronics and Applications*, Vol. 13, No. 2, 34, 2023.

[20] Khedr, A. A., B. E. Elnaghi, and A. M. Mohamed, "Design of a compact dual port 2 × 1 ultra-wideband MIMO antenna for radio frequency energy harvesting based on four "a" shaped slots," *Progress In Electromagnetics Research M*, Vol. 128, 41–49, 2024.

[21] Kim, S.-J., S. Kim, J.-H. Lee, and J.-W. Yu, "A compact broadband stepped bow-tie antenna for ambient RF energy harvesting," *IEEE Access*, Vol. 11, 60 365–60 373, 2023.

[22] El-Hakim, H. A. and H. A. Mohamed, "Engineering planar antenna using geometry arrangements for wireless communications

and satellite applications," *Scientific Reports*, Vol. 13, No. 1, 19196, 2023.

[23] El-Hakim, H. and H. A. Mohamed, "Synthesis of a multiband microstrip patch antenna for 5G wireless communications," *Journal of Infrared, Millimeter, and Terahertz Waves*, Vol. 44, No. 9, 752–768, 2023.

[24] Balanis, C. A., *Antenna Theory: Analysis and Design*, John Wiley & Sons, 2016.

[25] Kunwar, A., A. K. Gautam, and K. Rambabu, "Design of a compact U-shaped slot triple band antenna for WLAN/WiMAX applications," *AEU — International Journal of Electronics and Communications*, Vol. 71, 82–88, 2017.

[26] Paul, L. C., S. C. Das, T. Rani, S. M. Muyeen, S. A. Shezan, and M. F. Ishraque, "A slotted plus-shaped antenna with a DGS for 5G sub-6 GHz/WiMAX applications," *Heliyon*, Vol. 8, No. 12, e12040, 2022.

[27] Pandey, U., P. Singh, R. Singh, V. Kumar, K. Ray, S. Mallik, H. M. Alshahrani, E. Elshiekh, M. Abbas, and B. O. Soufiene, "Ultra-wideband microstrip folded antenna for wireless LAN, 5G and Internet of Things applications," *Scientific Reports*, Vol. 14, No. 1, 29319, 2024.

[28] Vaid, S. and A. Mittal, "High gain planar resonant cavity antennas based on metamaterial and frequency selective surfaces," *AEU — International Journal of Electronics and Communications*, Vol. 69, No. 9, 1387–1392, 2015.

[29] Yang, L., Y. J. Zhou, C. Zhang, X. M. Yang, X.-X. Yang, and C. Tan, "Compact multiband wireless energy harvesting based battery-free body area networks sensor for mobile healthcare," *IEEE Journal of Electromagnetics, RF and Microwaves in Medicine and Biology*, Vol. 2, No. 2, 109–115, 2018.

[30] Muncuk, U., K. Alemdar, J. D. Sarode, and K. R. Chowdhury, "Multiband ambient RF energy harvesting circuit design for enabling batteryless sensors and IoT," *IEEE Internet of Things Journal*, Vol. 5, No. 4, 2700–2714, 2018.

[31] Afify, Y. M., A. Allam, H. Kanaya, and A. B. Abdelrahman, "High-efficiency dual-band rectifier using coupled-line matching for RF energy harvesting applications," *Progress In Electromagnetics Research C*, Vol. 161, 255–260, 2025.

[32] Pandey, R., A. K. Shankhwar, and A. Singh, "An improved conversion efficiency of 1.975 to 4.744 GHz rectenna for wireless sensor applications," *Progress In Electromagnetics Research C*, Vol. 109, 217–225, 2021.

[33] Polaiah, G., K. Krishnamoorthy, and M. Kulkarni, "Compact high-efficiency pentahedron and quatrefoil shape antennas with enhanced gain for GSM1800, 3G, 4G-LTE energy harvesting applications," *International Journal of Microwave and Wireless Technologies*, Vol. 13, No. 3, 274–285, 2021.

[34] Rashwan, Y. R., A. S. A. El-Hameed, G. M. Dousoky, and E. Tammam, "Design of an efficient 2.45 GHz antenna array for RF energy harvesting," *SVU-International Journal of Engineering Sciences and Applications*, Vol. 5, No. 2, 175–183, 2024.